Mechatronic Systems and Control, Vol. 53, No. 10, 2025
An Open Access Paper

A MILLING CHATTER DETECTION METHOD BASED ON WPD AND O-VMD

Jingjing Gao,* Xinli Yu,* Bo Liu,* and Jing Liu*

Abstract

The relationship between dynamic characteristics and chatter recognition of machine tool spindle system was established based on dynamic characteristics and wavelet packet. After signal decomposition and acquisition of dynamic characteristics, signal recombination was carried out. The chatter was detected by wavelet packet decomposition and variational mode decomposition based on particle swarm optimisation algorithm, and the validity of parameter optimisation scheme was verified by experiments. The multi-scale permutation entropy feature is used to identify the machining state, which can distinguish the machining state at different time scales, so as to identify the chatter.

Key Words

Wavelet packet decomposition (WPD), variational mode decomposition (VMD), feature extraction, multiscale permutation entropy

1. Introduction

Chatter is a common phenomenon in mechanical processing, which can cause a decrease in surface quality. It is very important to detect chatter in a timely manner during mechanical processing and take certain proactive measures, such as changing processing parameters to avoid the occurrence of chatter. Accurately extracting chatter features is an important component of online monitoring. However, due to the complex processing environment and the time-varying characteristics of system characteristics, it is not easy for workers to detect chatter in the early stages of occurrence, but chatter has already had an irreversible impact on the processing system. In recent years, research on chatter identification has been widely carried out [1].

Time domain analysis, also known as waveform analysis, directly analyses the original sequence of signals. Ye *et al.* [2] computed the time-domain sequence's root mean square and identified chatter using the coefficient of variation, which is the ratio of the standard deviation to the mean of the root mean square sequence. While the time-domain analysis method is easy to understand and straightforward, in real-world machining, the dynamic properties of tools and workpieces can result in nonlinear and non-stationary signals that are easily disrupted by outside signals. Frequency domain analysis, also known as spectral analysis, occurs when a chatter occurs, the amplitude of the signal undergoes significant changes, and the peak of the chatter frequency occurs near the natural frequency. Rumusanu *et al.* [3] employed the fast fourier transform (FFT) to compute the ratio of the highest amplitude to the average value of the frequency domain physical signal, and used this value to assess the processing system's stability. During cutting, Tang [4] monitored chatter using the force signal's power spectrum density (PSD). However, chatter signals are frequently nonlinear and unstable, and standard FFT based spectrum analysis is only appropriate to stationary signal analysis, resulting in poor robustness.

In order to address the aforementioned issues, chatter detection employs adaptive signal decomposition techniques like empirical mode decomposition (EMD) [5], ensemble EMD (EEMD) [6]–[8], wavelet transform (WT) and its improved algorithm [5], [9], [10], variational mode decomposition (VMD) [11], [12]. Litak *et al.* [13] used time–frequency analysis techniques, such as wavelet analysis and Hilbert Huang transform (HHT) based on the milling force that gradually changes the cutting depth during the milling process of chromium nickel iron alloy, in an attempt to find chatter characteristics during the changing process. Karam and Teti [14] used a combination of force sensor detection and wavelet decomposition signals for feature extraction and style recognition research on the chip morphology of turning 1045 carbon steel. The findings of the experiment demonstrate that the wavelet-decomposed data feature vector can increase the neural decision-making system's recognition chip shape's accuracy. Fu *et al.* [6] first decomposed the signal into EMD; then, select the intrinsic mode components (IMF) with the highest energy proportion based on the energy limit coefficient. Finally, the HHT was used to the IMF to produce the HHT time spectrum [30], [31]. Chatter was determined by calculating the HHT time spectrum's normalised energy ratio and coefficient of variation. Although EMD has many advantages, it is actually prone to modal confusion, so it is rarely applied in chatter monitoring. In response to this defect, Norden E. Huang *et al.* [15] proposed the

* School of Mechanical Engineering, Liaoning Petrochemical University, Fushun 113001, China; e-mail: {gjj_913, yxl19820229, liubo981218, make_75}@163.com.
Corresponding author: Xinli Yu

Recommended by Simon X. Yang
(DOI: 10.2316/J.2025.201-0518)

EEMD method based on EMD. Ji *et al.* [7] used the two EEMD indicators of fractal dimension and PSD to track the milling state. Then used morphological coverage and the Fourier transform, respectively, to derive the equations for fractal dimension and PSD. The test results proved that the spectrum analysis results were consistent with the change trend of fractal dimension curve and PSD curve. Liu *et al.* [8] processed the original signal using set EMD, collecting energy entropy (EE) and sample entropy (SE) from the intrinsic mode function to separate chatter. VMD is a new non recursive signal processing method [15]. Once VMD was proposed, it was widely used in the field of fault monitoring. Reference [16] points out that the VMD method is more accurate in extracting the features of vibration signals. Aneesh *et al.* [17] compared and analysed the methods of combining VMD and EWT with SVM, indicating that VMD and SVM methods are more effective. Zhang *et al.* [18] proposed a chatter identification method based on the combination of VMD decomposition and EE.

Given the aforementioned benefits, VMD is frequently employed in chatter research; however, in signal processing, the number of decomposition layers and penalty factors must be predetermined. The accuracy of chatter signal decomposition is directly impacted by parameter selection. Yang *et al.* [19] suggested optimising variational modal decomposition for chatter monitoring by maximising the numeber of decomposition layers and penalty factors through the use of a simulated annealing approach. In order to identify chatter, the reconstructed signal's estimated entropy and SE are taken out, and the energy ratio is utilised as the criterion for choosing sub signals during the monitoring phase. The effects of manually setting VMD parameters are avoided with this strategy. To efficiently deconstruct the original signal and acquire the chatter frequency range, Liu *et al.* [20] used the FFT spectrum to choose the number of decomposition layers. Despite being a popular new technique for chatter monitoring, VMD still needs more research to determine the best mix of decomposition layers and penalty components.

The right feature must be chosen as the benchmark for chatter vibration detection in order to identify chatter in the real machining process. Based on the Hilbert–Huang spectrum, Liu *et al.* [5] developed an efficient chatter detection indicator that calculated the instantaneous frequency's mean and standard deviation and set its characteristic thresholds at 710 Hz and 0.02 Hz, respectively. Nevertheless, this method's threshold value will also vary depending on the cutting conditions, and its universality is weak. Currently, the selection of chatter features mostly concentrates on certain features that are derived from the idea of entropy, such as, permutation entropy (PE) [11], EE [21], SE [7], [8] , PSD [23], *etc.* These characteristics are appropriate for various processing situations and are chatter sensitive. Wavelet decomposition before VMD is a strategy that combines two signal processing techniques. The main purpose is to improve the accuracy and robustness of signal analysis. This method is effective in dealing with complex signals, especially signals containing non-stationary and multi-scale features.

Based on the above issues, this article proposes a milling chatter monitoring method based on wavelet packet decomposition (WPD) and optimised VMD decomposition. The specific research approach is as follows: Firstly, the signal to be analysed is decomposed using wavelet packets. Sub signals with abundant chatter information are chosen for reconstruction based on energy feature calculations. Perform mutual verification between the wavelet packet time–frequency map and the energy proportion of each node. However, the particle swarm optimisation (PSO) algorithm is applied to the reconstructed signal to make the choice of VMD decomposition parameters more scientific. The reconstructed signal is subjected to optimised VMD decomposition, the EE features of each order of IMF are calculated, and the Hilbert spectrum is used to verify the effectiveness of extracting chatter frequency bands. Finally, the multi-scale arrangement entropy was calculated as a chatter feature, and the entropy values of three different processing states were compared. The research process of this article is shown in Fig. 1

2. Mathematical Model of Chatter Detection Scheme

2.1 WPD

If $x(t)$ is a finite energy function, *i.e.,* $f(t) \in L^2(R)$, then the WT of this function is defined as an integral transform with the function family $\psi_{a,b}(t)$ as the integral kernel [22]–[24], as follows:

$$W_f(a,b;\psi) = \int_{-\infty}^{\infty} f(t)\psi_{a,b}(t)\mathrm{dt}, a > 0 \tag{1}$$

Assuming $\{\mu_n(x) \mid n \in Z_+\}$ is an orthogonal wavelet packet relative to filter h_n, and the coefficient of $f(x)$ in subspace U_j^n is $\left\{c_k^{j,n} \mid k \in Z\right\}$, it can be expressed as:

$$c_k^{j,n} = \int_{-\infty}^{\infty} f(x)2^{j/2}\mu_n\left(2^j x - k\right)\mathrm{dx} \tag{2}$$

Then the coefficients of $f(x)$ in subspaces U_{j-1}^{2n} and U_{j-1}^{2n+1} are $\left\{c_p^{j-1,2n}\right\}$ and $\left\{c_p^{j-1,2n+1}\right\}$:

$$c_p^{j-1,2n} = \sum_l h(l-2k)c_l^{j,n} \tag{3}$$

$$c_p^{j-1,2n+1} = \sum_l g(l-2k)c_l^{j,n} \tag{4}$$

Where, h_n—Low pass filter, g_n—High pass filter.

2.2 PSO

The decomposition accuracy of VMD is always constrained by the selection of decomposition layers and penalty factors, and improper parameter combinations may lead to VMD decomposition failure. Therefore, this paper proposes to use PSO algorithm, which was proposed by Dr. Eberhart and Dr. Kennedy [25] in 1995. The fundamental idea is derived from the regularity of bird swarm activity,

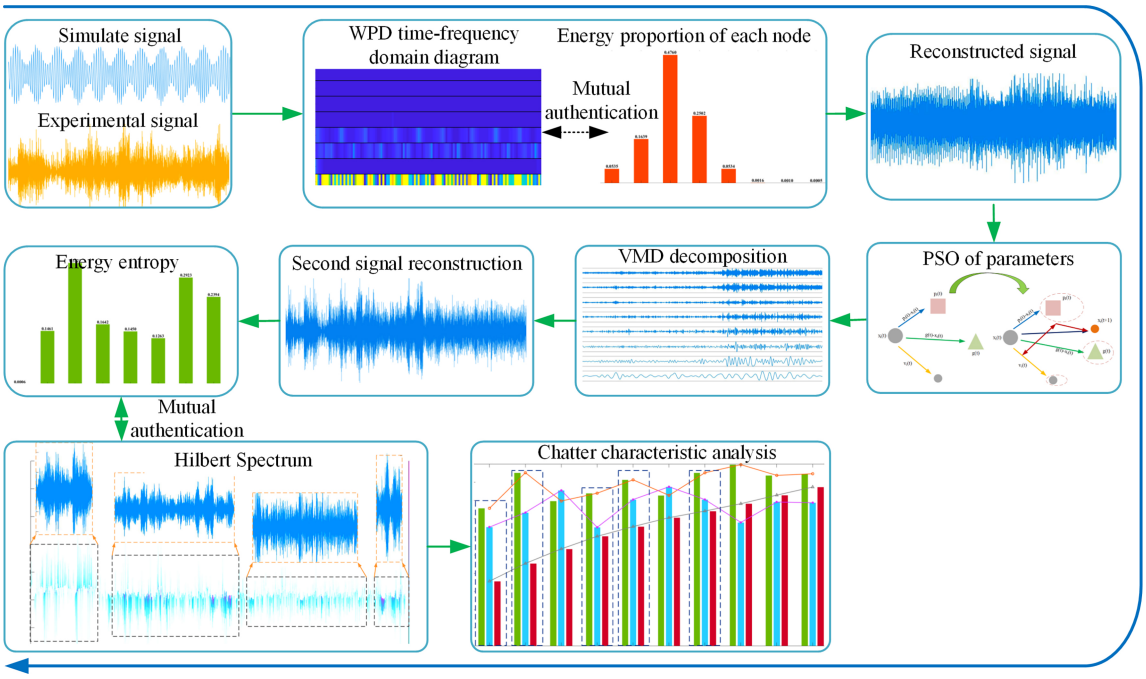

Figure 1. Chatter detection scheme.

and a swarm intelligence method is used to construct a mathematical model.

In the process of using the PSO to find the optimal solution, each particle will combine other individuals and their own information to find the optimal solution. Each particle learns the population's historical ideal value g_{best} and the individual's historical optimal value p_{best}. Each particle will adjust its speed and position according to these two optimal values, and the quality of each position is determined by the optimisation function, that is, the fitness function. In this article, the maximisation of the EE mean of IMFs is used as the optimisation function. The optimisation ends when the maximum value remains constant or when the maximum number of iterations is reached.

A population is made up of N particles in a D-dimensional search space, each of which is a D-dimensional vector, and its spatial position can be represented as:

$$x_i = (x_{i1}, x_{i2}, \ldots, x_{\mathrm{iD}}), i = 1, 2, \ldots, N \tag{5}$$

The current fitness value can be calculated by bringing it into the fitness function, and the current optimisation result can be measured according to the size of the fitness value. The global historical optimal position of all particle swarm is as follows:

$$g_{\mathrm{besti}} = (g_{\mathrm{baeti\ 1}}, g_{\mathrm{besti2\ 2}}, \ldots g_{\mathrm{bestiD}}), i = 1, 2, \ldots, N \tag{6}$$

The velocity update expression of the particle swarm is as follows:

$$\begin{aligned} v_{\mathrm{ij}}(t+1) = {} & v_{\mathrm{ij}}(t) + c_1 r_1 \left(p_{\mathrm{bestij}}\ (t) - x_{\mathrm{ij}}(t)\right) \\ & + c_2 r_2 \left(g_{\mathrm{bestij}} - x_{\mathrm{ij}}\right) \end{aligned} \tag{7}$$

The position update expression is as follows:

$$x_{\mathrm{ij}}(t+1) = x_{\mathrm{ij}}(t) + v_{\mathrm{ij}}(t+1) \tag{8}$$

Where, j-the j-th dimension of particles, i-i-th particle, t-current iterations, c_1-individual learning factors, c_2-group learning factor, r_1,r_2-independent parameters.

The schematic diagram and algorithm flowchart of the body steps are shown in Fig. 2.

2.3 VMD

The principle of VMD is that any signal can be composed of a set of sub-signals with a specific centre frequency and limited bandwidth. These sub-signals are called IMF. The VMD algorithm realises the decomposition of the signal through the construction and solution of the variational problem. Based on the signal's adaptive properties, the non-recursive approach can automatically calculate the necessary number of modes and the centre frequency.

The advantage of VMD is that compared with the traditional EMD, the VMD algorithm has better noise robustness and stronger theoretical basis. Its modal components are more closely around their respective centre frequencies, avoiding the problem of modal aliasing.

Decomposing a real input signal f into a discrete number of sub signals (modes) u_k with distinct sparsity qualities at input time is the aim of variational modal decomposition. In order to evaluate the bandwidth of a modality, the following scheme is proposed [15]:

The square norm of the demodulated signal's gradient is used to estimate the bandwidth. The constrained

variational problem can be described as:

$$\min_{\{u_k\},\{\omega_k\}} \left\{ \sum_k \partial_t \left[\left(\delta(t) + \frac{j}{\pi \mathrm{t}} \right) * u_k(t) \right] e^{-j\omega_k t}{}_2^2 \right\} \quad s.t. \sum_k u_k = f. \tag{9}$$

Where, $\{u_k\} = \{u_1, \ldots, u_k\}$ and $\{\omega_k\} = \{\omega_1, \ldots, \omega_k\}$ are the sets of modal and central frequencies, respectively. Similarly, $\sum_k = \sum_K^{k=1}$ are the sum of all modes.

Reconstructed constraints can be treated with different schemes. For the problem to become unrestricted, the quadratic penalty term and Lagrange multiplier λ are used simultaneously, which can be calculated with the following formula:

$$\begin{aligned} &L\left(\{u_k\}, \{\omega_k\}, \lambda\right) \\ &= \alpha \sum_k \partial_t \left[\left(\delta(t) + \frac{j}{\pi \mathrm{t}} \right) * u_k(t) \right] e^{-j\omega_k t}{}_2^2 \\ &\quad + f(t) - \sum_k u_k(t)_2^2 + \lambda(t), f(t) - \sum_k u_k(t) \end{aligned} \tag{10}$$

An iterative optimisation process called the alternate direction multiplier method (ADMM) uses the answer of the initial minimisation problem formula (11) as a saddle point. The steps to solve the saddle point using ADMM are as follows:

$$\begin{aligned} u_k^{n+1} = \underset{u_{k\in X}}{\operatorname{argmin}} \Big\{ &\alpha \partial_t \left[\left(\delta(t) + \tfrac{j}{\pi \mathrm{t}} \right) * u_k(t) \right] e^{-j\omega_k t}{}_2^2 \\ &+ f(t) - \textstyle\sum_i u_i(t) + \frac{\lambda(t)}{2}{}_2^2 \Big\} \end{aligned} \tag{11}$$

The solution to the quadratic optimisation problem is easy to find, allowing the positive frequency of the first change to disappear, resulting in modal updates:

$$\widehat{u}_k^{n+1}(\omega) = \frac{\widehat{f}(\omega) - \sum_{i \neq k} \widehat{u}_i(\omega) + \frac{\widehat{\lambda}(\omega)}{2}}{1 + 2\alpha \left(\omega - \omega_k\right)^2} \tag{12}$$

By using the above equation, the Wiener filtering of the current residual and the initial value $1/(\omega\text{-}\omega_k)^2$ of the signal can be calculated. Then, due to Hilbert's symmetry, the spectrum of the modes can be completed.

The bandwidth prior knowledge is utilised to optimise the centre frequency in order to acquire it, and further optimisation can be carried out based on the definition of average frequency. The specific process can be described as: introducing the ADMM algorithm to solve the optimisation results, combining with Fourier domain transformation, and finally obtaining the decomposition results of variational modal decomposition.

2.4 Multi-scale PE

Bandt and Pompe [26] introduced the concept of PE, a technique for tracking time series' randomness and dynamic mutation behaviour. Its benefits include easy computation, quick speed, robust noise resistance, and suitability for online monitoring. In mechanical fault monitoring as well as other domains, it has been widely used.

The set of time series PE values at various scales is known as MPE, and the following is how it is calculated [27]:

The j-th reconstruction component of the time series X reconstruction matrix is shown in (13), where $j_1, j_2 j_3, \ldots, j_m$ represents the column coordinates of each element in the reconstruction component.

$$\begin{aligned} x\left(i + (j_1 - 1)\tau\right) &\leqslant x\left(i + (j_2 - 1)\tau\right) \\ &\leqslant \cdots \leqslant x\left(i + (j_m - 1)\tau\right) \end{aligned} \tag{13}$$

In m-dimensional phase space mapping, different symbol sequences share $m!$. A sequence of symbols arranged in different ways. Calculate the probability P_1,P_2,... P_k of the occurrence of each symbol sequence, wherein time series X's PE of k distinct symbol sequences is defined as follows:

$$H_p(m) = -\sum_{m!}^{j=1} P_j \ln P_j \tag{14}$$

Where, $0 \leqslant H_p(m) \leqslant ln(m!)$, when P_j=1/$m!$, $H_p(m)$ has a maximum value ln($m!$). Normally, $H_p(m)$ is normalised, *i.e.,*:

$$H_p = H_p(m)/ln(m!) \tag{15}$$

The time series $X = \{x(i), i = 1, 2, \ldots, N\}$ is coarse–grained, and each coarse–grained time series is calculated by the following formula:

$$y_j^{(\tau)} = \frac{1}{\tau} \sum_{\mathrm{j}\tau}^{i=(j-1)\tau+1} x_i, j = 1, 2, \ldots N/\tau \tag{16}$$

Where, τ represents the scale factor, N/τ represents the length of the coarse–grained time series.

Multiscale PE analysis is the process of calculating the PE of the current scale factors after the original time series has been coarse-grained by time scale factors.

3. Simulation Analysis and Experimental Verification

With the introduction of concepts, such as intelligent machine tools and intelligent workshops, traditional machining has shifted towards intelligence and artificial direction, and milling plays an important role in it [28]. The machining of thin-walled components, such as aircraft engine blades is prone to regenerative chatter due to their low stiffness characteristics during the machining process. At present, chatter is a key factor affecting high-precision and high-efficiency machining, and online monitoring of milling chatter has become increasingly important. This article will combine WPD and O–VMD to detect the occurrence of milling chatter. Firstly, simulation signals will be used to verify the proposed scheme. After obtaining feasible results, an experimental platform will be built to demonstrate the robustness of the method.

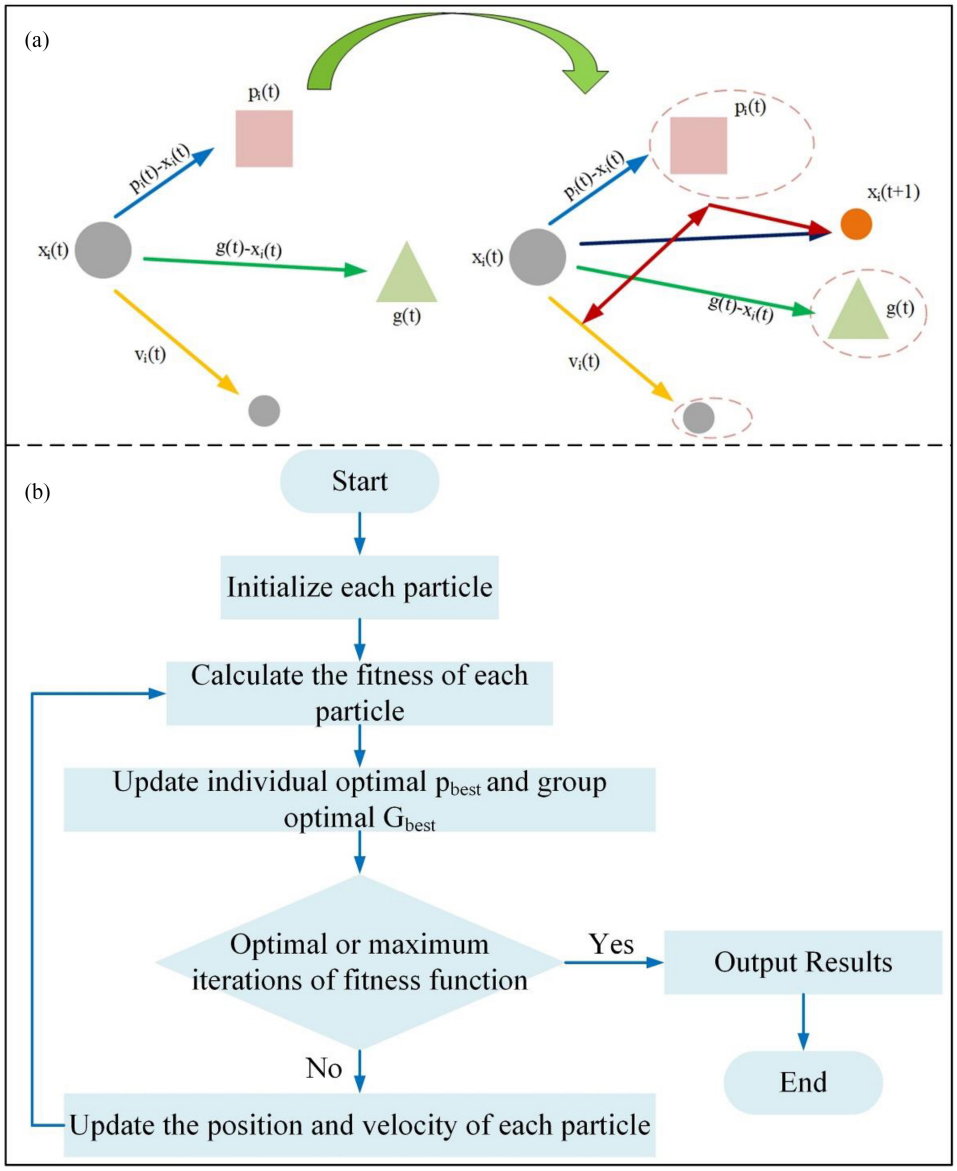

Figure 2. Schematic diagram of PSO steps and algorithm flow chart: (a) Schematic diagram of PSO steps; and (b) Algorithm flow chart.

3.1 Simulation Signal Analysis

To validate the proposed method, simulation signal analysis was conducted in this section. The physical signal during the occurrence of chatter is simulated as:

$$\begin{aligned} y_1 &= 4 \times \sin(86\pi t) \\ y_2 &= 5 \times \sin(45\pi t) \\ y_3 &= 0.8 \times (1 + 0.5\sin(36\pi t)) \\ &\quad \times \cos(360\pi t + 2.4 \times \sin(18\pi t)) \end{aligned} \tag{17}$$

Among them, y_1 and y_2 are the fundamental and octave frequencies of the spindle speed frequency of the simulation signal, as well as the fundamental and octave frequencies of the tooth pass frequency. y_3 is the chatter signal frequency range of the simulation signal

The simulation signal y is

$$y = y_1 + y_2 + y_3 \tag{18}$$

The amplitude and phase modulation components are introduced as the third component, as modulation is a common mode found in chatter signals. The simulated chatter signal and its three components are shown in Fig. 3, respectively. The figure displays the simulated chatter signal's spectrum. It is evident that the chatter frequency band's amplitude is much smaller than the periodic signal's.

After proving that the constructed simulation signal contains rich chatter information, WPD will be performed on the simulation signal to extract sub signals with rich chatter information. At the same time, signal denoising can also be achieved. Due to the absence of noise in the simulation signal, the physical signal in actual processing contains noise. When chatter occurs, the energy of the chatter frequency will increase sharply, which will lead to signal reconstruction. Following the computation of each node's energy *via* WPD, select wavelet packet nodes with higher energy values for signal reconstruction.

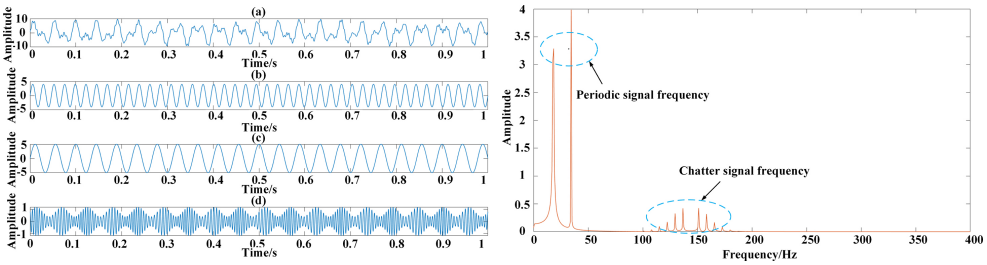

Figure 3. Time domain waveform and Frequency domain waveform: (a) simulation signal; (b) and (c) periodic signal; (d) simulation chatter signal.

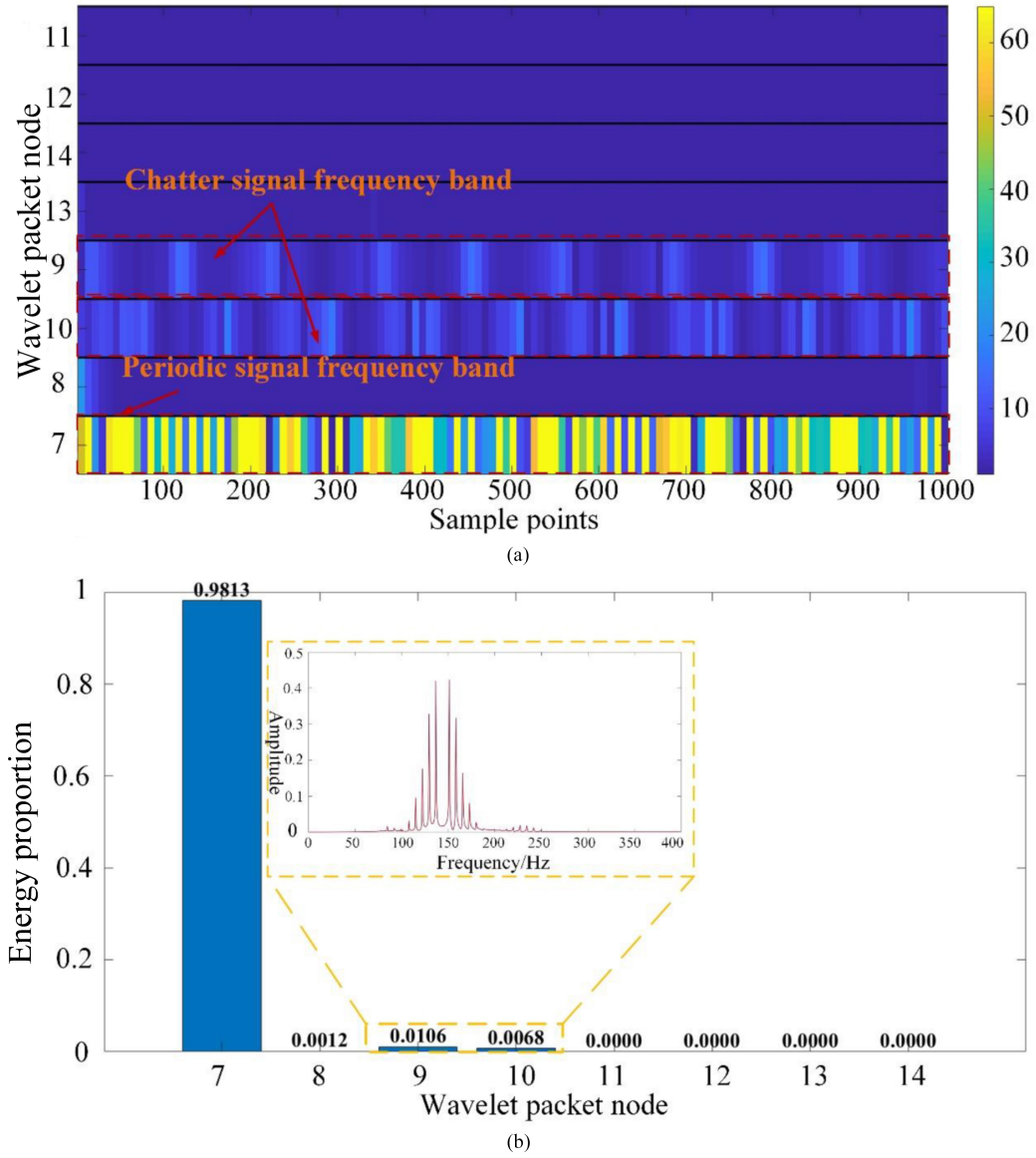

Figure 4. Time frequency domain diagram of wavelet packet nodes and energy ratio of each node of wavelet packet.

WPD is used to extract chatter frequency bands for signal reconstruction. For three-layer WPD, "Demy" is employed as a wavelet basis function. The signal frequency bands of nodes 7–14 are 0–50 *Hz*, 50–100 *Hz*, 100–150 *Hz*, 150–200 *Hz*, 200–250 *Hz*, 250–300 *Hz*, 300–350 *Hz* 350–400 *Hz*, respectively.

From Fig. 4, it can be clearly seen that wavelet packet node seven is a periodic frequency band in the original signal, with a higher amplitude; wavelet packet nodes nine and 10 are the chatter frequency bands in the original signal, with relatively small amplitudes. Next, determine each node's energy characteristics within the wavelet packet in order to pick the reconstructed sub

Table 1
PSO Initialisation Parameters

Number of Initial Population	Spatial Dimension	Maximum Number of Iterations	Decomposition Level Optimisation Range	Penalty Factor Optimisation Range
500	2	10	[2,10]	[500,3500]
Decomposition layer speed limit	Penalty factor speed limit	Self-learning factor	Group learning factor	Inertia weight
[0,0]	[−10,10]	0.5	0.5	0.8

signals. seven nodes represent the energy ratio of the periodic signal in the original signal, while nine and 10 nodes represent the energy ratio of the chatter signal in the original signal. Reconstruct signals from nine nodes and 10 nodes to obtain time-domain waveforms. This reconstruction scheme retains rich chatter information and filters out periodic signals. The denoising characteristics of WPD will also be presented in subsequent experiments.

The accuracy of variational modal decomposition is always constrained by the setting of the decomposition layers and penalty factors. Improper selection of decomposition parameters can easily lead to the failure of VMD decomposition, resulting in endpoint effects and modal aliasing, which affects subsequent feature extraction. Therefore, this paper will use PSO to globally optimise the decomposition levels and penalty factors. The PSO algorithm's initialisation parameter settings are displayed in Table 1.

This article uses the maximum average energy of IMFs as the optimisation function. Figure 5 shows the three-dimensional scatter plot of PSO. It can be seen from Fig. 5(b) that the marked optimisation results have significantly higher average energy of IMFs than other results. To prove the effectiveness of this optimisation result, it is decomposed as an input parameter for VMD decomposition, and the distribution of its time domain and frequency spectrum is analysed. From Fig. 6, it can be seen that the frequency distribution is clear. There was no modal aliasing, and the peak frequency was consistent with the simulation signal setting. Therefore, this parameter optimisation scheme is effective.

To calculate chatter characteristics more accurately, identify machining states, and reconstruct signals, VMD is performed. The modes and spectra of each order are shown in Fig. 6. The amplitude of the IMF1 waveform in Fig. 6 is small and there are peaks at low frequencies. This part is a frequency band independent of the chatter frequency, therefore, to fully select the chatter frequency band, the signal will be reconstructed for the second time. Fault monitoring makes extensive use of EE, which is an extension of energy in the entropy domain. The EE of each order of IMFs will be calculated.

The EE properties of each order of IMFs are displayed in Table 2. Similar to the previous analysis, there is no rich chatter information in IMF1. Therefore, IMF2 and IMF3 will be subjected to a second signal reconstruction. At the same time, Table 3 calculated the numerical characteristics of the two sets of signals before and after reconstruction,

Table 2
EE Characteristics

Components of each order of IMFs	1	2	3
Energy entropy	0.0001	0.3662	0.3662

Table 3
Numerical Characteristics of Two Groups of Signals

	Raw Signal	Second Reconstruction Signal
Average value	−1.9593e-4	−1.8348e-4
Variance	0.3590	0.3406
Standard deviation	0.5992	0.5836

verifying the feasibility of the second reconstruction scheme.

Based on the above analysis, the sub signals rich in chatter information have been reconstructed. Zhixue [29] extracted chatter features based on the reconstructed signal MPE. In this section, multi-scale arrangement entropy features will be used to identify the processing state. We compared the entropy values of the stable part, slight chatter, and severe chatter parts in the simulation signal at different scales.

From Fig. 7, it can be seen that under the time scale of the dashed line in the figure, the milling processing state, stable, slight vibration, and severe vibration can be clearly distinguished with distinct boundaries. However, at other scales, there has been confusion in the processing status, making it difficult to identify the processing status. Starting from the concept of multi-scale, it can be found that when the time series is small, coarsening will cause the original time series to shorten, thereby affecting the characteristics of the time series, resulting in little difference in calculated PE values, and thus affecting state recognition.

3.2 Experimental Analysis

The robustness of the chatter monitoring scheme will be demonstrated by milling experiments. The milling experiment is carried out in a CNC machining centre,

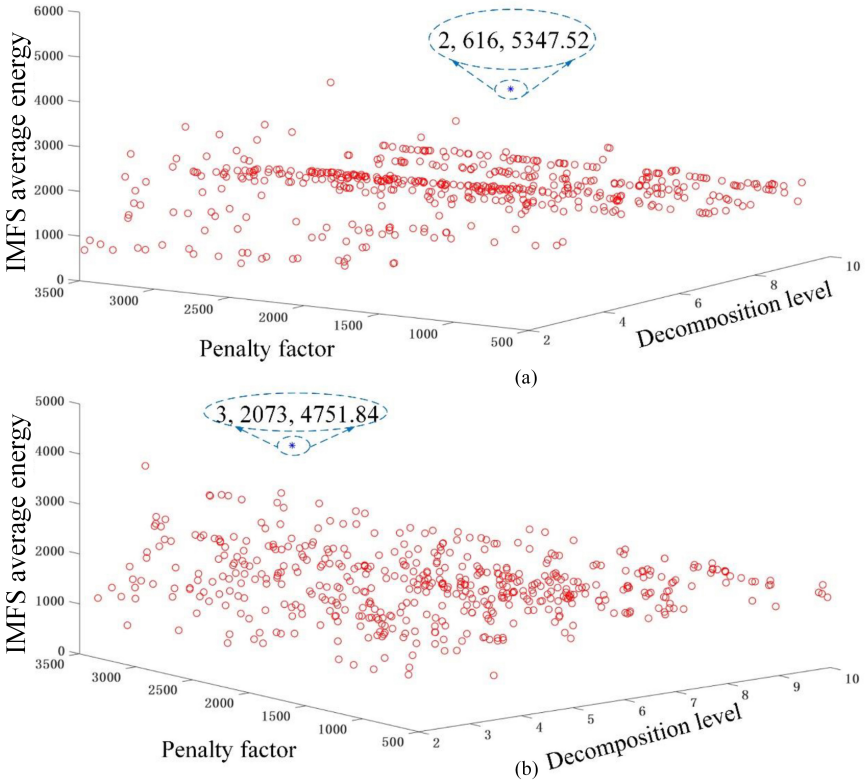

Figure 5. PSO.

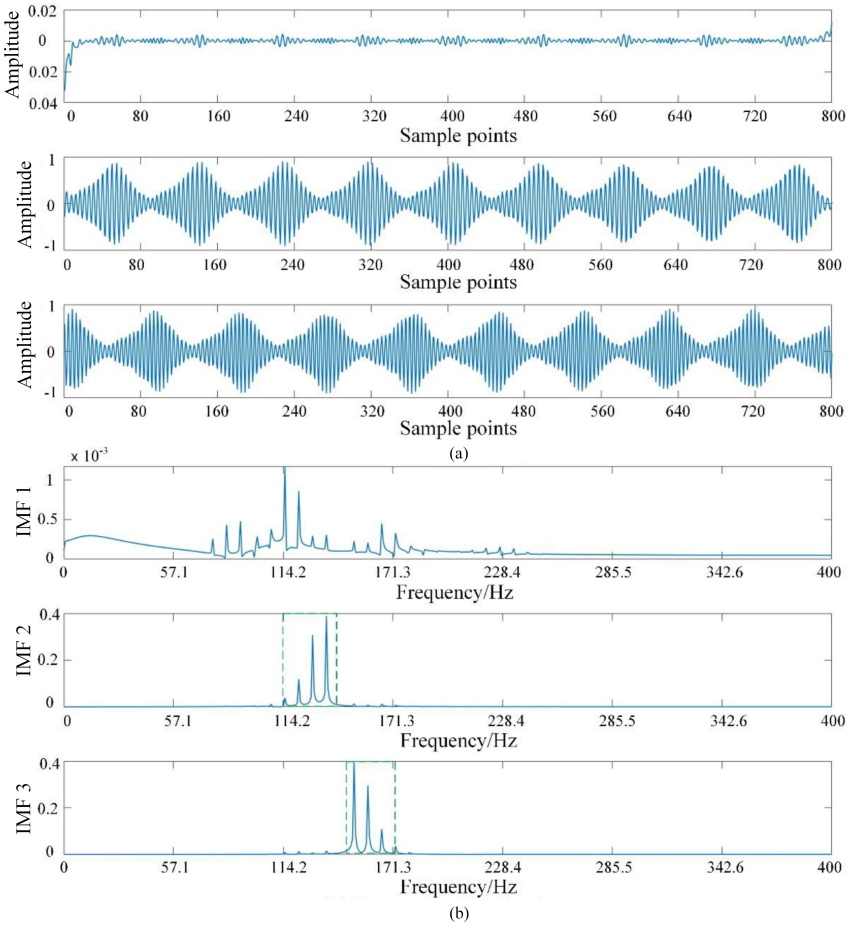

Figure 6. VMD decomposition: (a) Time domain diagram of each order of IMFs; and (b) corresponding frequency domain diagram.

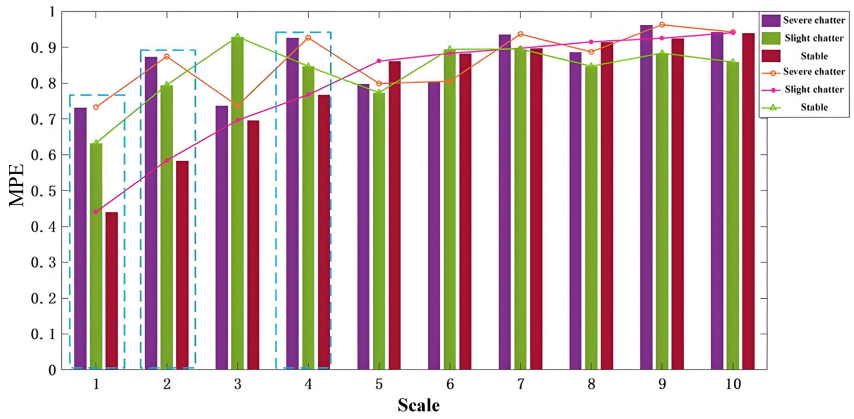

Figure 7. Chatter characteristics.

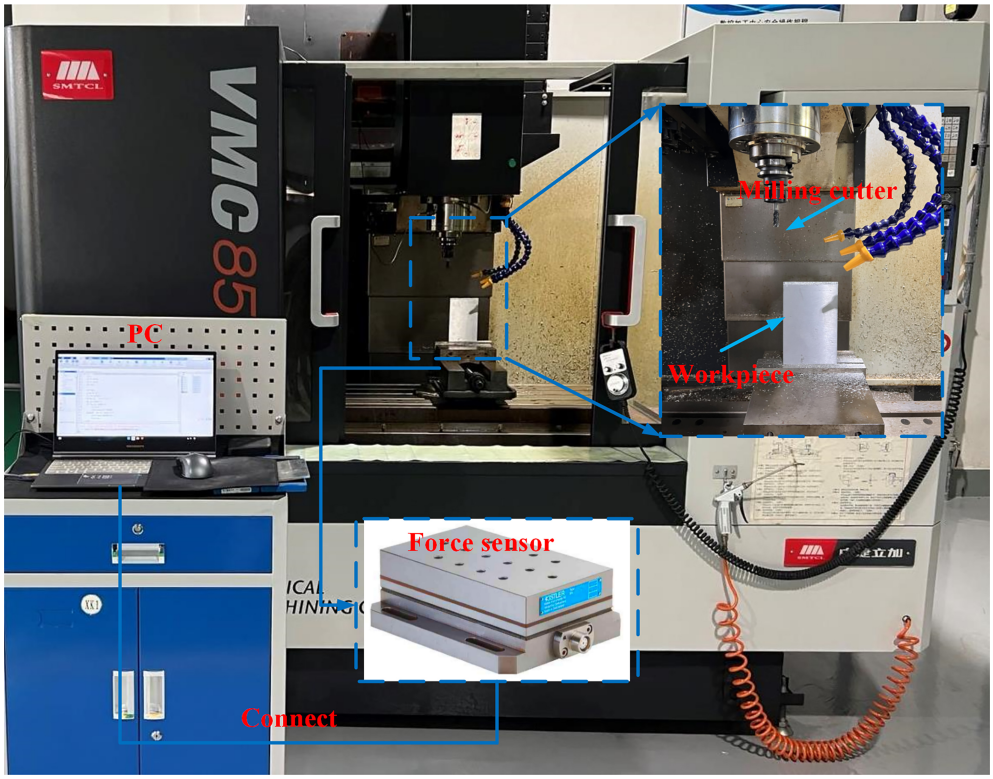

Figure 8. Experimental setup.

and the specific experimental setup is shown in Fig. 8. The experimental equipment was a four axis *VMC850E* machining centre, and experiments were conducted under dry milling conditions. The workpiece material is made of aluminium alloy *Al6061*, with a size of *150* mm × *150* mm × *5* mm. The processing parameters are shown in Table 4.

The experimental sequence number (4) will be used for flutter monitoring analysis, and Fig. 9 shows the time-domain and frequency-domain waveforms of this signal segment.

From the time-domain image in Fig. 9, it can be clearly seen that the difference between the chattering part and the stable part is that the cutting force increases significantly when chattering occurs, while the cutting force is relatively small when stable machining occurs. Although time-domain features can distinguish processing states, due to the instantaneous and nonlinear characteristics of chatter occurrence, time-domain methods are difficult to capture chatter occurrence in real-time. The chatter frequency peak in the frequency domain will be close to the system's inherent frequency; nevertheless, variations in noise and the dynamic properties of the system may cause errors. Therefore, this article proposes a time-frequency domain monitoring chatter scheme. Firstly, to denoise and obtain subsignals containing rich chatter information, the original signal is subjected to WPD. Then, VMD decomposition is performed on the reconstructed signal, and finally, chatter frequency bands are extracted to calculate chatter characteristics. Similar to the analysis of

Table 4
Milling Parameters

Experiment Number	Axial Cutting depth/mm	Radial Cutting depth/mm	Spindle speed/rpm	Feed speed/mm/min
1	3	0.6	1200	150
2	3	0.9	1200	150
3	5	0.6	1200	150
4	5	0.9	1200	150

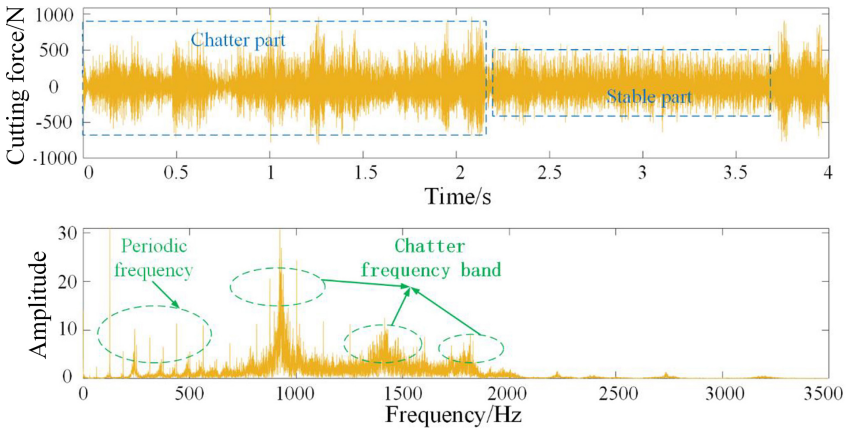

Figure 9. Processing signal.

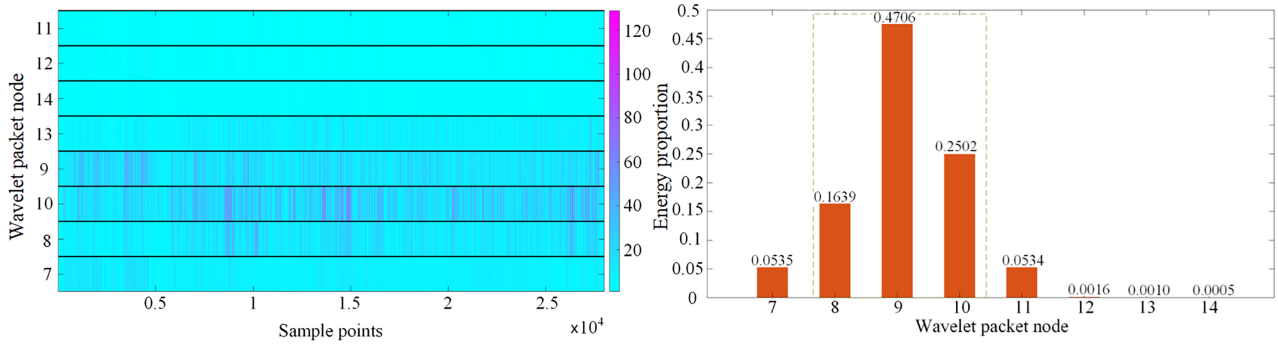

Figure 10. Energy of each node of WPD.

simulated signals, the "Demy" wavelet was selected as the wavelet basis function for three-layer WPD. The signal frequency bands of nodes 7–14 are 0–437.5 *Hz*, 437.5–875 *Hz*, 875–1312.5 *Hz*, 1312.5–1750 *Hz*, 1750–2187.5 *Hz*, 2187.5–2625 *Hz*, 2625–3062.5 *Hz*, and 3062.5–3500 *Hz*, respectively. The energy of each node in WPD is shown in Fig. 10.

In Fig. 10, energy is gathered in nodes eight, nin, and 10, and it is preliminarily determined as a chatter frequency band. To verify this judgement, the energy proportion of each wavelet packet node is calculated, and based on this, the chatter frequency band is extracted for signal reconstruction. Calculating chatter characteristics, distinguishing processing status, and reconstructing the time-domain and frequency-domain waveforms of the signal as shown in Fig. 11.

In Fig. 11, it is evident that the reconstructed signal accomplishes the goals of noise reduction and periodic component removal while retaining the information of the chatter frequency band in the frequency domain. In the simulation signal analysis, the same results were obtained, so the signal reconstruction scheme is feasible. The spectrum distribution shows a total of four frequency bands A, B, C, and D. According to the description in the references [20], the number of decomposition layers of VMD can be determined by the number of frequency bands. However, the physical signal actually collected may contain some interference information, so this paper uses it as a reference to verify with PSO algorithm. Same as the analysis of simulation signal, VMD parameter optimisation is carried out for the reconstructed signal to find the optimal combination of decomposition parameters.

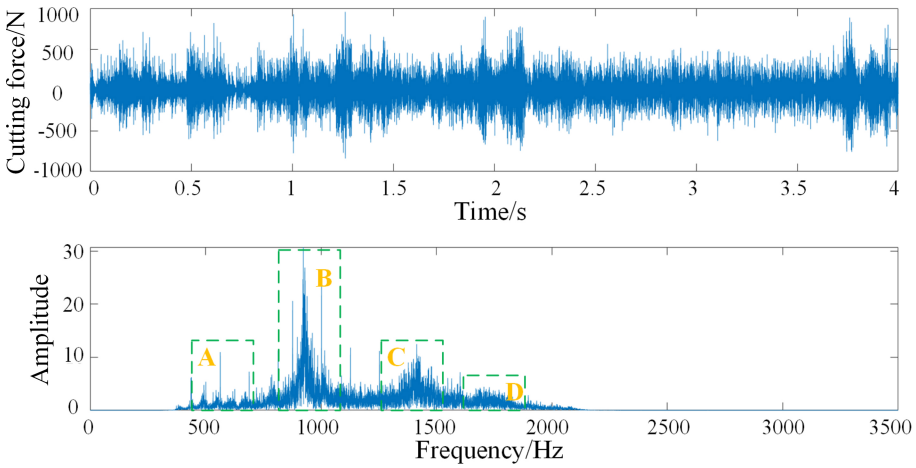

Figure 11. Time domain and frequency domain diagram of reconstructed signal.

Table 5
PSO Initialisation Parameters

Number of Initial Population	Spatial Dimension	Maximum Number of Iterations	Decomposition Level Optimisation Range	Penalty Factor Optimisation Range
500	2	10	[2,10]	[500,3500]
Decomposition layer speed limit	Penalty factor speed limit	Self-learning factor	Group learning factor	Inertia weight
[0,0]	[−10,10]	0.5	0.5	0.8

The initialisation parameters of PSO are shown in Table 5.

Figure 12 shows the PSO for the above reconstructed signal. The optimisation result of the final state is consistent with the above judgement. To further verify, compare the spectrum distribution of the IMF in the final state with the initial state, as shown in Fig. 13.

In Fig. 13(a), the spectrum distribution of the reconstructed signal is the same, with peak distributions of four frequency bands present, without modal aliasing. However, in Fig. 13(b), multiple frequency bands are mixed together in both the first-order IMF and the second IMF, resulting in VMD decomposition failure. This will result in incomplete chatter information in the reconstructed signal and affect the extraction of chatter features.

To calculate chatter characteristics more accurately, the reconstructed signal will be subjected to optimised VMD decomposition, and the EE feature will be applied to the second signal reconstruction, extracting frequency bands with high energy chaos as sub signals for the chatter characteristics to be analysed. In Fig. 14, the reconstructed signal was subjected to VMD decomposition, obtaining the time-domain and spectral distribution of various levels of IMFs. However, the accuracy of VMD decomposition is limited by the setting of the decomposition layers and penalty factors. Therefore, the current decomposed sub signals cannot be subjected to chatter feature analysis. In this article, the EE properties of each order of IMFs are calculated, the chatter frequency band is identified based on the EE value, and signal reconstruction is carried out.

Table 6
EE Characteristics

Components of each order of IMFs	1	2	3	4
Energy entropy	0.0015	0.2804	0.1628	0.3298

From Table 6, it can be seen that IMF2, IMF3, and IMF4 have a high degree of energy chaos and high EE values, indicating complex frequencies within their frequency bands. Therefore, signal reconstruction was performed on this third-order IMF. In order to verify the accuracy of the reconstructed signal, Hilbert spectrum was used to analyse the reconstructed signal.

Figure. 15 shows the Hilbert transform of the reconstructed signal. The graphic illustrates that the reconstructed signal contains a wealth of chatter information in addition to retaining a large amount of the original signal's content. In the figure, each signal segment in the time domain can correspond to the time–frequency image. This further proves the feasibility of the proposed signal reconstruction scheme. In order to compare the entropy values under various processing states, the multi-scale arrangement entropy features of the reconstructed signal are computed.

In Fig. 16, the processing state is divided into three states: stable processing, slight vibration, and severe vibration. The higher the entropy value, the more unstable

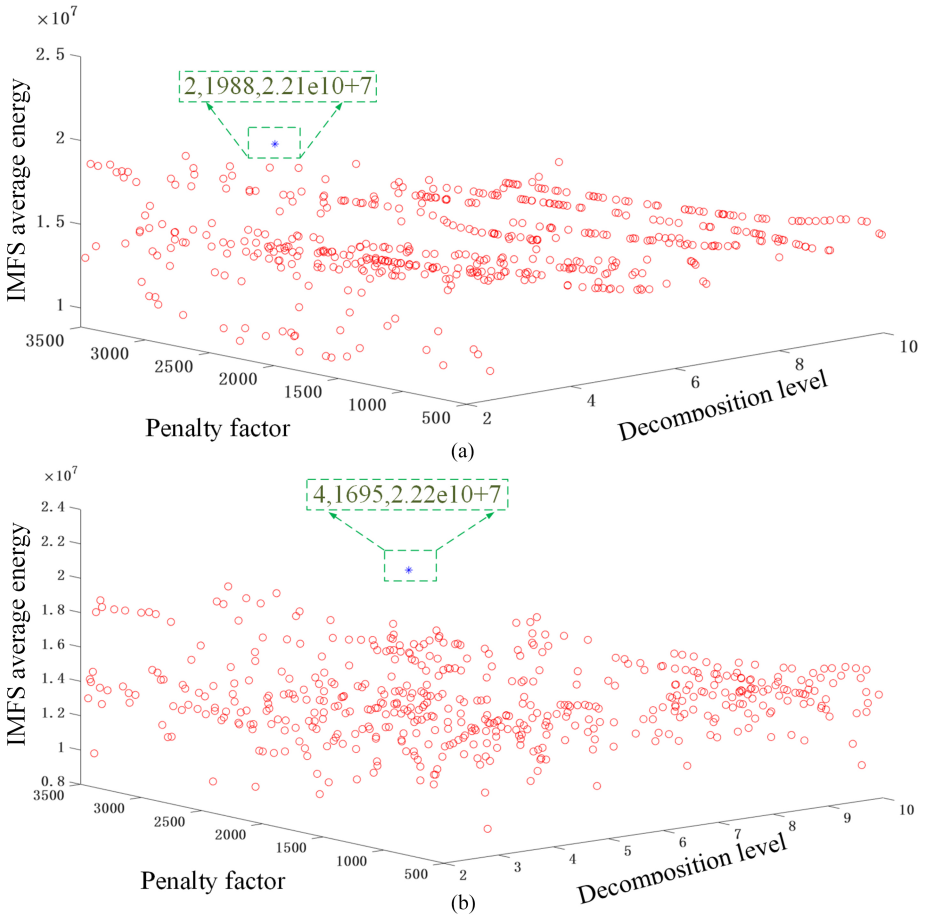

Figure 12. PSO of experimental signal.

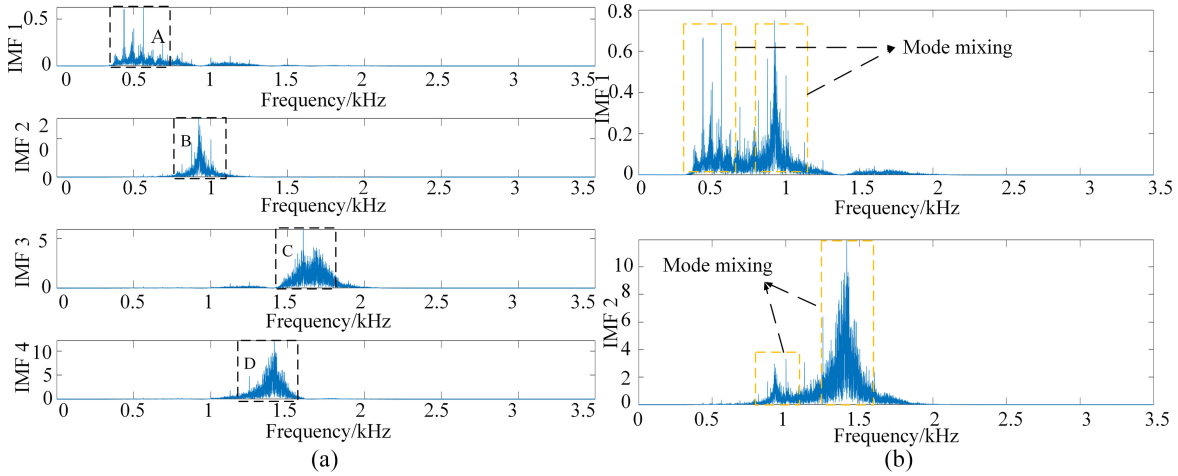

Figure 13. Effect of the spectral distribution of decomposition layers.

the processing state is. The introduction of the multi-scale concept enables a single entropy feature to exhibit different entropy values at different time scales, thereby increasing the robustness of discriminating processing states. The dashed box in the figure indicates that the machining status can be accurately identified at this scale. In simulation signal analysis, due to the short time series, coarse-grained calculations can lead to inaccurate entropy values, resulting in fewer effective scales. In the experimental signal, the sampling frequency is 7000 Hz and the sampling time is 4 s. Therefore, the sample points of the original time series to be analysed are 28000. The effective scale rises in tandem with multi-scale PE. This also proves the conjecture that there are fewer effective scales when analysing simulated signals. Multi scale arrangement entropy can effectively distinguish processing states, with high computational efficiency, strong adaptability of entropy features in time and frequency domains, and is not affected by processing

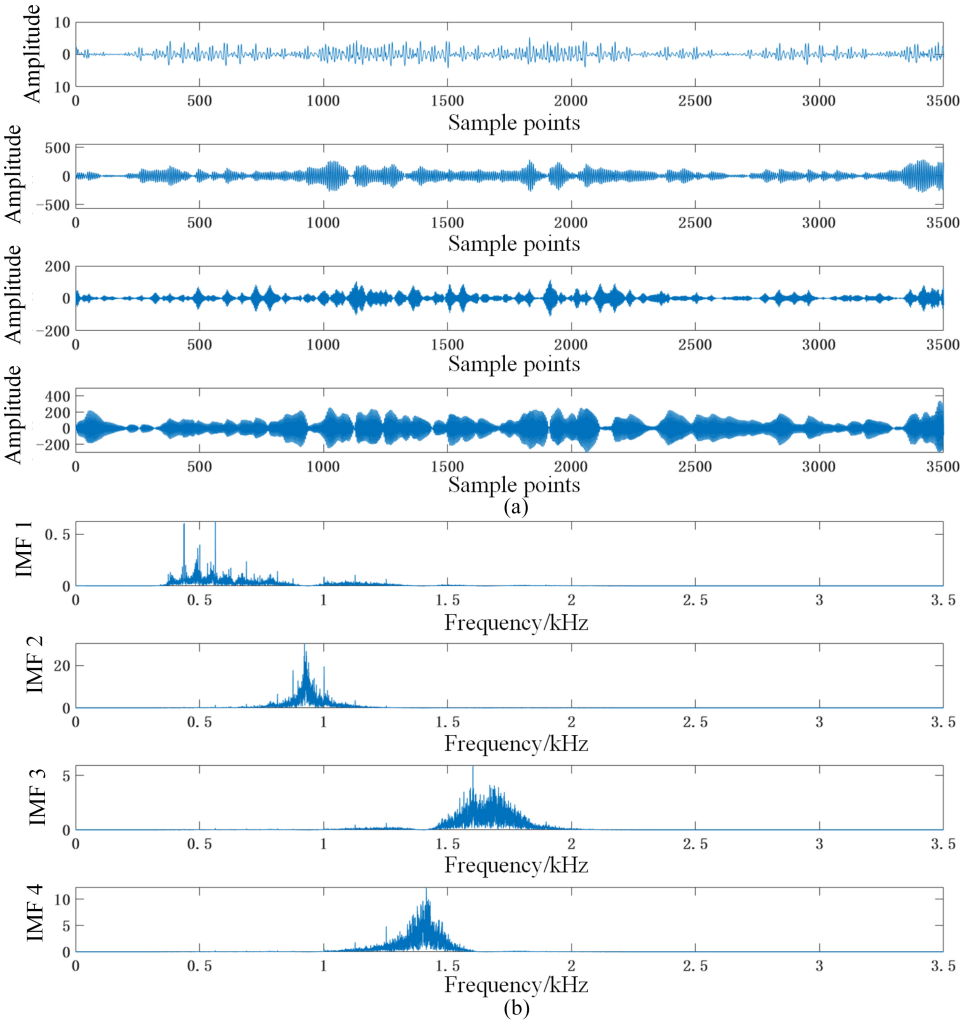

Figure 14. VMD decomposition of reconstructed signal.

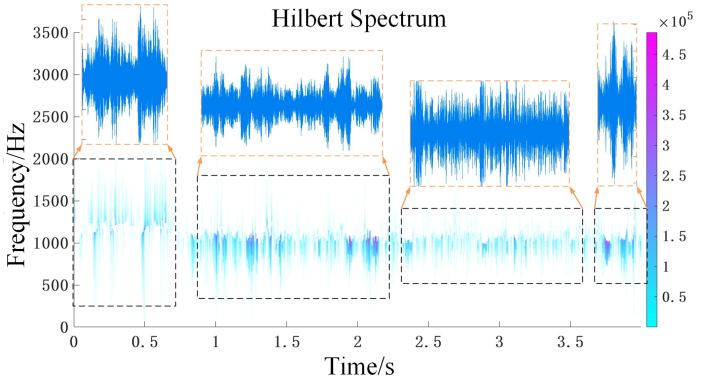

Figure 15. Hilbert transform.

parameters. The histogram and line chart in Fig. 16 fully demonstrate the effectiveness of the proposed chatter monitoring scheme.

4. Conclusion

WPD and variational modal decomposition based on PSO algorithm are proposed in this paper. The feasibility of this scheme has been confirmed by simulation signals and experimental signals. WPD exhibits good performance in extracting target frequency bands and denoising, and compares the effects of different decomposition levels on VMD decomposition results. Choosing the appropriate K value cannot easily lead to modal aliasing. Then the reconstructed signal is implemented with PSO, and the results of optimised parameters are mutually verified with the spectrum and wavelet packet energy distribution of the reconstructed signal. The results prove

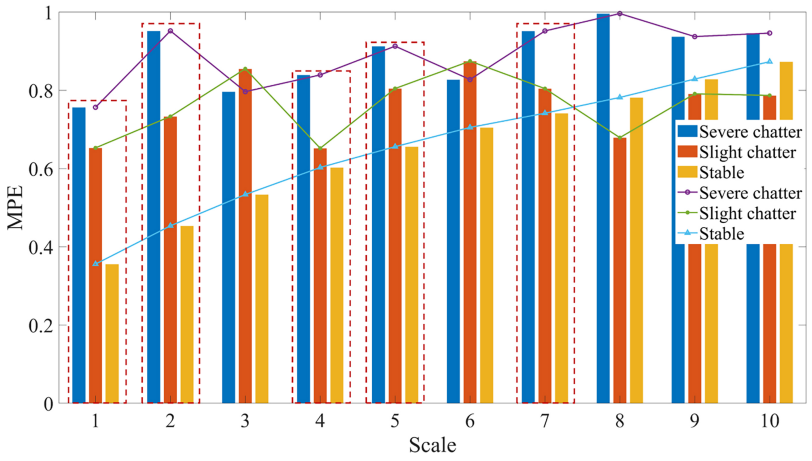

Figure 16. Chatter characteristics.

the effectiveness of the parameter optimisation scheme. Finally, the chatter characteristics, namely, the multi-scale arrangement entropy, are calculated. The simulation and experimental results indicate that multi-scale arrangement entropy can distinguish processing states and identify chatter at different time scales.

5. Acknowledgements

The work was supported by Basic Scientific Research Project of Liaoning Provincial Department of Education (No. JYTMS20231456).

References

[1] G. Quintana and J. Ciurana, Chatter in machining processes: A review, *International Journal of Machine Tools & Manufacture*, *51*(5), 2011, 363–376.

[2] J. Ye, P. Feng, C. Xu, Y. Ma, and S. Huang, A novel approach for chatter online monitoring using coefficient of variation in machining process, *International Journal of Advanced Manufacturing Technology*, *96*(1), 2018, 287–297.

[3] G.R. Frumusanu, I.C. Constantin, V. Marinescu, and A. Epureanu, Development of a stability intelligent control system for turning, *International Journal of Advanced Manufacturing Technology*, *64*(5–8), 2013, 643–657.

[4] S. Tangjitsitcharoen, In-process monitoring and detection of chip formation and chatter for CNC turning, *Journal of Materials Processing Technology*, *209*(10), 2009, 4682–4688.

[5] C. Liu, L. Zhu, and C. Ni, The chatter identification in end milling based on combining EMD and WPD, *International Journal of Advanced Manufacturing Technology*, *91*(9–12), 2017, 3339–3348.

[6] Y. Fu, Y. Zhang, H. Zhou, D. Li, H. Liu, H. Qiao, and X. Wang, Timely online chatter detection in end milling process, *Mechanical Systems and Signal Processing*, *75*, 2016, 668–688.

[7] Y. Ji, X. Wang, Z. Liu, Z. Yan, L. Jiao, D. Wang, and J. Wang, EEMD-based online milling chatter detection by fractal dimension and power spectral entropy, *The International Journal of Advanced Manufacturing Technology*, *92*(1–4), 2017, 1185–1200.

[8] L. Zhu, C. Liu, C. Ju, and M. Guo, Vibration recognition for peripheral milling thin-walled workpieces using sample entropy and energy entropy, *The International Journal of Advanced Manufacturing Technology*, *108*(6), 2020, 3521–3266.

[9] H. Cao, Y. Lei, and Z. He, Chatter identification in end milling process using wavelet packets and Hilbert–Huang transform *International Journal of Machine Tools and Manufacture*, *69*, 2013, 11–19.

[10] Q. Zhang, X. Tu, F. Li, and Y. Hu, An effective chatter detection method in milling process using morphological empirical wavelet transform *IEEE Transactions on Instrumentation and Measurement*, *69*(8), 2019, 5546–5555.

[11] K. Li, S. He, B. Luo, B. Li, H. Liu, and X. Mao, Online chatter detection in milling process based on VMD and multiscale entropy, *The International Journal of Advanced Manufacturing Technology*, *105*(12), 2019, 5009–5022.

[12] X. Li, S. Wan, X.W. Huang, and J. Hong, Milling chatter detection based on VMD and difference of power spectral entropy, *The International Journal of Advanced Manufacturing Technology*, *111*(7), 2020, 2051–2063.

[13] G. Litak, K. Kecik, and R. Rusinek, Cutting force response in milling of Inconel: Analysis by wavelet and Hilbert-Huang transforms, *Latin American Journal of Solids & Structures*, *10*(1), 2013, 133–140.

[14] S. Karam and R. Teti, Transform feature extraction for chip form recognition during carbon steel turning, *Procedia Cirp*, *12*, 2013, 97–102.

[15] K. Dragomiretskiy and D. Zosso, Zosso dominique.variational mode decomposition, *IEEE Transactions on Signal Processing*, *62*(3), 2014, 531–544.

[16] Y. Wang, R. Markert, J. Xiang, and W. Zheng, Research on variational mode decomposition and its application in detecting rub-impact fault of the rotor system, *Mechanical Systems & Signal Processing*, *60–61*, 2015, 243–251.

[17] C. Aneesh, S. Kumar, P.M. Hisham, and K.P. Soman, Performance comparison of variational mode decomposition over empirical wavelet transform for the classification of power quality disturbances using support vector machine, *Procedia Computer Science*, , *46*, 2015, 372–380.

[18] Z. Zhang, H. Li, G. Meng, X. Tu, and C. Cheng, Chatter detection in milling process based on the energy entropy of VMD and WPD, *International Journal of Machine Tools & Manufacture*, , *108*, 2016, 106–112.

[19] K. Yang, G. Wang, Y. Dong, Q. Zhang, and L. Sang, Early chatter identification based on an optimised variational mode decomposition, *Mechanical Systems and Signal Processing*, *115*, 2019, 238–254.

[20] L. Changfu and J. J. Qiu, Chatter feature extraction method for variable depth of cut side milling based on VMD and FFT, *Journal of Northeastern University*, *39*(8), 2018, 92–96.

[21] Z. Zhi, L. Chengying, L. Xinjun, and Z. Jie, Analysis of milling vibration state based on the energy entropy of WPD, *Journal of Mechanical Engineering*, *54*(21), 2018, 57–62.

[22] Z.K. Peng and F.L. Chu, Application of the wavelet transform in machine condition monitoring and fault diagnostics: A review with bibliography, *Mechanical Systems and Signal Processing*, *18*(2), 2004, 199–221.

[23] T.P. Le and P. Paultre, Modal identification based on continuous wavelet transform and ambient excitation tests, *Journal of Sound and Vibration*, *331*(9), 2012, 2023–2037.

[24] Z. Nenadic and J.W. Burdick, Spike detection using the continuous wavelet transform, *IEEE Transactions on Biomedical Engineering*, *52*(1), 2004, 74–87.
[25] R. Eberhart and J. Kennedy, A new optimizer using particle swarm theory, in *Proceedings of the 6th International Symposium on Micro Machine and Human Science*, 1995, 39–43.
[26] C. Bandt and B. Pompe, Permutation entropy: A natural complexity measure for time series, *Physical Review Letters*, , *88*(17), 2002, 174102.
[27] G. Ouyang, C. Dang, and X. Li, *Analysis of EEG Data with Multiscale Permutation Entropy*, (Dordrecht: Springer),2011, 741–745.
[28] Y. Quan, C. Liu, Z. Yuan, and B. Yan, Hybrid data augmentation combining screening-based MCGAN and manual transformation for few-shot tool wear state recognition, *IEEE Sensors Journal*, , *415*(12), 2024,12186–12196.
[29] W. Zhixue, *Research on Online Evolutionary Identification Method and Suppression Technology of Chatter in Side Milling of Thin-Walled Parts-D*, Harbin University of Science and Technology, Harbin, 2022. DOI: https://dx.doi.org/10.27063/d.cnki.ghlgu.2022.000002
[30] Q. Wang and X. Wang, A fault detection diagnosis predict O bserver based on resource allocation network, *Mechatronic Systems and Control, 50*(2), 2022, 96–101. DOI: https://dx.doi.org/10.2316/J.2022.201-0277
[31] J. Si, Y. Cao, and X. Shi, , Fault diagnosis of wind turbine planetary gearbox based on HHT and structure resonance demodulation, *Mechatronic Systems and Control*, *47*(1), 2019, 36–42. DOI: https://dx.doi.org/10.2316/J.2019.201-2966

Biographies

Jingjing Gao was born in 1983 in Qinhuangdao, Hebei Province, China. She received the master's degree in mechanical manufacturing and automation from Liaoning Petrochemical University in July 2011. Since 2011, she has been a Teacher with Liaoning Petrochemical University. Her research interests include mechanical processing stability and chip surface integrity.

Xinli Yu was born in 1982, in Dandong, Liaoning Province, China. She received the Doctoral degree in mechanical manufacturing and automation from Liaoning Fuxin University in June 2023. Since 2014, she has been a Teacher with Liaoning Petrochemical University. Her research interests include tool wear monitoring and chatter detection.

Bo Liu was born in February 1998 in Changchun, Jilin Province, China. He received the master's degree in energy power and engineering from Liaoning Petrochemical University in July 2023. He is currently pursuing the Doctoral degree with Jilin University. His research interests include chatter detection and data-driven learning.

Jing Liu was born in July 1979, in Fushun, Liaoning Province, China. She received the master's degree in computational mathematics and computer applications from Liaoning Petrochemical University in July 2008. Since 2008, she has been a Teacher with Liaoning Petrochemical University. Her research interests include pattern recognition and machine health monitoring.